Primary role of suppressor of cytokine signaling 1 in *Mycobacterium bovis* BCG infection

Shogo Soma,[a,b] Satoru Kawai,[c] Hiroyasu Inada,[d] Kenta Watanabe,[e] Satoru Mizuno,[a,f] Seiichi Kato,[b,f] Kazuhiro Matsuo,[f] and Yasuhiro Yasutomi[a,b]

[a]Department of Molecular and Experimental Medicine, Mie University Graduate School of Medicine, 2-174 Edobashi, Tsu, Mie 514-8507, Japan.

[b]Laboratory of Immunoregulation and Vaccine Research, Tsukuba Primate Research Center, National Institutes of Biomedical Innovation, Health and Nutrition, 1 Hachimandai, Tsukuba, Ibaraki 305-0843, Japan.

[c]Department of Tropical Medicine and Parasitology, Dokkyo Medical University, Mibu, Shimotsuga, Tochigi 321-0293, Japan

[d]Faculty of Pharmaceutical Science, Department of Pathology, Suzuka University of Medical Science, Minamitamagaki, Suzuka, Mie 513-8670, Japan.

[e]Joint Faculty of Veterinary Medicine, Laboratory of Veterinary Public Health, Yamaguchi University, 1677-1 Oaza Yoshida, Yamaguchi 753-8515, Japan

[f]Research and Development Department, Japan BCG Laboratory, 3-1-5 Matsuyama, Kiyose, Tokyo 204-0022, Japan.

Running title: Role of SOCS1 in BCG infection

22 Address correspondence and reprint requests to Dr. Yasuhiro Yasutomi, Laboratory of
23 Immunoregulation and Vaccine Research, Tsukuba Primate Research Center, National
24 Institutes of Biomedical Innovation, Health and Nutrition, 1 Hachimandai, Tsukuba, Ibaraki
25 305-0843, Japan.
26 Phone & Fax: (+81) 029-837-2053
27 E-mail address: yasutomi@nibiohn.go.jp.

ABSTRACT

Suppressor of cytokine signaling 1 (SOCS1) is a negative regulator of JAK/STAT signaling and is induced by mycobacterial infection. To understand the major function of SOCS1 during infection, we established a novel system in which recombinant Bacillus Calmette-Guérin expressed dominant-negative SOCS1 (rBCG-SOCS1DN) because it would not affect the function of SOCS1 in uninfected cells. When C57BL/6 mice and $Rag1^{-/-}$ mice were intratracheally inoculated with rBCG-SOCS1DN, the amount of rBCG-SOCS1DN in the lungs was significantly reduced compared to the amounts in the lungs of mice inoculated with a vector control counterpart and wild-type BCG. However, these significant differences were not observed in $Nos2^{-/-}$ mice and $Rag1^{-/-}Nos2^{-/-}$ double-knockout mice. These findings demonstrated that SOCS1 inhibits NO production to establish mycobacterial infection and the rBCG-SOCS1DN has the potential to be a powerful tool for studying the primary function of SOCS1 in mycobacterial infection.

INTRODUCTION

Suppressor of cytokine signaling 1 (SOCS1) is a negative regulator of JAK/STAT signaling. Although SOCS1 expression should be tightly regulated to avoid cytokine dysregulation while maintaining effective control of pathogens, SOCS1 is highly upregulated by infection with several pathogens. SOCS1 is thought to contribute to pathogen escape from the host protective cytokine production response (1-5) in *Mycobacterium* species including not only virulent strains but also the avirulent strain *Mycobacterium bovis* Bacillus Calmette Guérin (BCG) that induces SOCS1 expression (6-8). However, SOCS1 function in mycobacterial infection is still unclear. Because the SOCS1-deficient mice are normal at birth but exhibit growth inhibition and die within 3 weeks after birth, it is difficult to study for primary function of SOCS1 (9, 10). In previous studies, SOCS1 silencing was shown to improve mycobacterial clearance in host cells (11), and examination of tissue-specific SOCS1-deficient mice indicated that *Mycobacterium tuberculosis* (Mtb) control in macrophages was improved (6). However, the function of SOCS1 in Mtb-uninfected cells is not shown in SOCS1-deficient animals using genetic modification. To overcome this issue, we established a new recombinant BCG (rBCG) that expresses a SOCS1 antagonist (rBCG-SOCS1DN). We previously reported that a mutation of SOCS1 (F59D) in a kinase inhibitory region strongly enhanced cytokine-dependent JAK/STAT activation both *in vivo* and *in vitro* (12). SOCS1 expression, which is induced by rBCG-SOCS1DN infection, is inhibited by the SOCS1DN protein, without affecting SOCS1 levels in uninfected cells. Therefore, the primary function of SOCS1 could be elucidated.

Nitric oxide (NO) is an important antimicrobial effector in infections with intracellular pathogens. NO is required for host immunity against intracellular pathogens and has direct antimicrobial toxicity (13). JAK/STAT signaling initiates NO production by transcriptional and post-transcriptional mechanisms that enhance expression of inducible nitric oxide synthase (iNOS, also known as NOS2) (14). NO also plays an essential role in killing Mtb, as shown in previous studies using $NOS2^{-/-}$ mice in which infection with Mtb was associated with significantly higher susceptibility than was infection in wild-type C57BL/6 mice (15, 16). However, the relationship between NOS2 and SOCS1 in mycobacterial infection is not fully understood.

Here, rBCG-SOCS1DN was more easily controlled during infection, showing no more activation of adaptive immunity than that with a vector control (rBCG-pSO). When $NOS2^{-/-}$ mice were used, however, this difference disappeared, thereby indicating that SOCS1 induction by BCG infection contributed to evasion from the host innate immune system by inducing a remarkable microbicidal mechanism that functions by NO production. This is the first report that rBCG-SOCS1DN, which acts as a modulator of the host immune system, could be a new powerful tool for the study of host factors in infectious disease.

RESULTS

Recombinant BCG expressing SOCS1DN

To examine protein expression in SOCS1DN, we processed a cell lysate from rBCGs. Western blot analysis showed that SOCS1DN and the HA-tag were present only in rBCG-SOCS1DN (Fig. 1A). Growth curves were obtained by periodically determining CFU, and there was no significant difference between rBCG-pSO and rBCG-SOCS1DN (Fig. 1B). To confirm that induction of SOCS1 expression can be caused by rBCGs, as was previously reported, J774.1 cells were infected with rBCG-SOCS1DN or rBCG-pSO. SOCS1 gene expression with rBCGs was significantly higher at 6 h post infection than that in uninfected cells (Fig. 1C). To estimate the effects of SOCS1DN on JAK/STAT signaling, we obtained lysates of rBCG-infected cells. Higher STAT1 phosphorylation levels were found in rBCG-SOCS1DN-infected cells than in rBCG-pSO-infected cells (Fig. 1D). Thus, the growth of rBCG was not affected by SOCS1DN transformation, and the effect of SOCS1 induced by BCG infection was inhibited by the SOCS1DN protein, which was expressed as a secreted protein by rBCG-SOCS1DN (Fig. S1).

Analysis of the viability of rBCG in infected

To examine the function of SOCS1 for BCG growth *in vivo*, C57BL/6 and RAG1$^{-/-}$ mice were intratracheally inoculated with BCG Tokyo, rBCG-pSO, or rBCG-SOCS1DN. The number of CFUs of all mycobacteria strains gradually decreased in C57BL/6 mice. At 28 days after infection, the number of rBCG-SOCS1DN was significantly smaller than the number of other

BCGs (Fig. 2A). Interestingly, a significant reduction of bacterial CFUs in lung was also observed in RAG1$^{-/-}$ mice throughout the observation period, even though there was no reduction in the numbers of CFUs of BCG Tokyo and rBCG-pSO in RAG1$^{-/-}$ mice (Fig. 2B). Histopathological analysis of the lung showed that infiltration of immune cells of both rBCG-SOCS1DN and rBCG-pSO was increased at each time point. At 14 days after inoculation, inflammation of lung inoculated with rBCG-SOCS1DN had subsided compared to rBCG-pSO infection (Fig. 2C). Because rBCG-pSO was not significantly different from BCG Tokyo, it was used as a control strain for further experiments.

To explore the key factor contributing to the difference between rBCG-SOCS1DN infection and rBCG-pSO infection, we examined the cytokine and chemokine profiles in BALF. In RAG1$^{-/-}$ and C57BL/6 mice, various cytokines and chemokines were secreted in BALF, However, there was no significant difference between these rBCGs (Fig. 3A, B). Lungs from rBCG-infected mice were harvested and homogenates were also assayed, but there was no significant difference (Fig. S2). The rBCG-SOCS1DN was controlled even in RAG1$^{-/-}$ mice, which cannot produce mature T cells or B cells (Fig. 2A), and the function of SOCS1 is inhibited in infected cells by the molecule of SOCS1DN (Fig. 1D). Because these data showed that SOCS1DN lead to inhibition of immune responses under the condition of no adaptive immune responses, we focused to dendritic cells which are mycobacterial target cells and have only bacteriostatic ability in nature (17).

rBCG-SOCS1DN-infected BMmDCs show reduced cell damage

To examine the viability of rBCGs in infected cells, BMmDCs were infected with rBCG-SOCS1DN or rBCG-pSO. Similar to the results obtained from the *in vivo* assay, the number of rBCG-SOCS1DN CFU was significantly reduced compared to that of rBCG-pSO (Fig. 4A). BMmDCs infected with rBCGs were also tested for acid-fast staining, and the total numbers of bacteria were determined for each cell preparation. At 1 day and 3 days after infection, no difference between rBCGs was observed. However, the bacterial numbers of rBCG-SOCS1DN were less than those of rBCG-pSO at 7 days post infection, especially in cells infected with over 11 bacilli (Fig. 4B). To better understand the causative factors for this difference, BMmDCs infected with rBCGs were subjected to TEM analysis. At 3 days after infection, rBCG-SOCS1DN-infected BMmDCs were observed to have a higher density of cytoplasm and dendrites than that in rBCG-pSO-infected cells (Fig. 4C). To confirm the difference in cell viability, rBCG-infected cells were visualized by dead cell staining reagents and examined by microscopy or flow cytometry. In agreement with the results of TEM analysis, a larger number of dead cells was detected in rBCG-pSO-infected cells than in rBCG-SOCS1DN-infected cells by using Trypan Blue staining and a SYTOX AADvanced dead cell staining kit (Fig. 4D and E). FACS analysis showed a rightward shift of weak signal-positive cells, indicating increased membrane permeability, in rBCG-pSO-infected cells (Fig. 4E). In addition, greater LDH release, indicating rupture of the cell membrane as a result of necrosis, was detected in rBCG-pSO-infected cells than in rBCG-SOCS1DN-infected cells at 7 days after infection (Fig. 4F). These results suggested that induction of SOCS1 via BCG infection affects the viability of infected cells.

BCG infection inhibits the production of NO in BMmDCs

The supernatant of BMmDCs infected with rBCGs was analyzed for its cytokine and chemokine profiles, but no significant difference was found between rBCG-pSO and rBCG-SOCS1DN (Fig. 5A). Although the level of IL-10 expression was decreased in rBCG-SOCS1DN-infected cells, mRNA expression levels were not changed and downregulation of STAT3 phosphorylation was not observed (Fig. S3, S4). Since activated DCs have enhanced anti-bacterial capacities, including generation of reactive NO through NOS2 upregulation (13, 14, 18), we next focused on NO responses in rBCG-infected BMmDCs. In contrast to other analytes, NO release from and NOS2 gene expression in rBCG-SOCS1DN-infected cells were significantly greater than no release from and NOS2 gene expression in rBCG-pSO-infected cells (Fig. 5B, C). These results suggest that NO production via upregulation of NOS2 was inhibited by BCG infection and that this inhibitory effect was modulated by SOCS1 upregulation.

Analysis of SOCS1 function in RAG1$^{-/-}$NOS2$^{-/-}$ (DKO) mice

To determine whether the modulation of NO production by SOCS1 is an important factor for BCG infection, we generated RAG1$^{-/-}$NOS2$^{-/-}$ (DKO) mice, and the mice were intratracheally inoculated with rBCGs. At 14 days after infection, the number of CFU of rBCG-SOCS1DN was smaller than that for control BCGs in C57BL/6 mice, whereas a significant difference was not observed for NOS2$^{-/-}$ mice. The number of CFU for rBCG-SOCS1DN was also

significantly reduced in RAG1$^{-/-}$ mice compared to that for control BCG, while there was no significant difference between the number of CFU of rBCG-SOCS1DN and that of control BCG in DKO mice. However, these responses become more apparent at 28 days after infection (Fig. 6A). Taken together, these results revealed that SOCS1 regulated innate immune responses by suppressing NO production during the early phase of BCG infection.

NO function for BCG infection

To determine whether BCG inhibits NO production to promote survival of infected cells, BMmDCs were generated from NOS2$^{-/-}$ mice and co-cultured with rBCGs. Consistent with the results of the *in vivo* experiment, rBCG-SOCS1DN easily survived in NOS2$^{-/-}$ BMmDCs, and the significant difference in bacterial burden observed in NOS2$^{+/+}$ (C57BL/6) BMmDCs disappeared in NOS2$^{-/-}$ BMmDCs at 7 days after infection (Fig. 7A). The growth of rBCGs was inhibited in a NO donor supplied condition (Fig. S5). Although the colonies of rBCG-SOCS1DN from NOS2$^{+/+}$ BMmDCs were very small compared to those of rBCG-pSO, the colonies of rBCG-SOCS1DN from NOS2$^{-/-}$ BMmDCs seemed to be similar to those of rBCG-pSO (Fig. 7B). These findings demonstrated that BCG infection may modulate NOS2 gene expression by SOCS1 induction for its survival in the first cells that BCG makes contacts with.

DISCUSSION

SOCS1 has been thought to negatively regulate protective immunity, given the association between gene expression during mycobacterial infection and severity of TB disease (6, 7, 19). Since the role of SOCS1 in mycobacterial infection is not well understood, attempts have been made in some studies to elucidate its function. However, the methodology used in those studies had a major limitation: SOCS1-deficient mice exhibited growth inhibition and died within 3 weeks after birth, showing excess acceleration of immune responses (9, 10). To address this issue, we constructed rBCG-SOCS1DN, which can provide an antagonist to compete with intrinsic SOCS1 in infected cells only. It could also be applicable to C57BL/6 mice, which could not be used to assess SOCS1 function because there were no methods available until now. Surprisingly, rBCG-SOCS1DN was eliminated not only in C57BL/6 mice but also in RAG1$^{-/-}$ mice, as demonstrated in both *in vivo* and *in vitro* experiments in which the essential players of adaptive immunity were shown not to be involved. Our results suggest that induction of SOCS1 by BCG infection contributes to the survival of BCG in the cells that they first make contact with. Although rBCG-SOCS1DN, which lacks an ESX-1 locus, can modulate the host JAK/STAT signal pathway (Fig. 1 and S2), the mechanism by which a secreted protein is transferred is still unclear. One possible mechanism is that other ESX genes, which can form a secretion system similar to that of ESX-1, are intact (20-22), and SOCS1DN molecules might be transferred to the cytoplasm.

There are two types of antigen (Ag)-presenting cells in the lungs, macrophages and dendritic cells, and both types of cells can phagocytose mycobacteria. Additionally,

appropriate innate and adaptive immune responses against mycobacterial infection were shown to require dendritic cell activation (11, 23-25). One mechanism of innate immune defense against mycobacteria involves production of NO from the NOS2 gene (18). NO synthesis is activated by cytokines, microbial compounds, or both, and these signaling cascades are modulated by SOCS1 molecules (26). Although the NOS2 gene is known to be upregulated in response to Mtb infection, it only exerts a bacteriostatic effect (27). In fact, rBCG-SOCS1DN were controlled in bone marrow-derived macrophages similar to BMmDC (Fig. S6); however, the differences were not so drastic. This might be due to the difference between macrophages and dendritic cells in innate bactericidal capacity (17). The enhancement of NOS2 gene expression controlled by Mtb might not be enough to generate a sufficient amount of NO to kill Mtb. In our study, BMmDCs infected with rBCGs showed higher levels of NO release and NOS2 gene expression than those in naïve cells, and these changes were promoted by rBCG-SOCS1DN infection. Therefore, induction of SOCS1 by BCG infection may cause inhibition of NOS2 gene expression and subsequent NO release in the innate immune system.

Cell damage caused by mycobacterial infection was reported to be biased towards necrosis, which is associated with the survival and virulence of the mycobacterial strain (28-31). In addition, NO activation contributes to the induction of apoptosis in host cells (18). In fact, rBCG-SOCS1DN has a minimal influence on host cell damage, and rBCG-SOCS1DN viability is affected by NOS2 expression and NO release levels, being consistent with our findings.

There are many known NOS2 inducers including IFN-αβ, IFN-γ, TNF-α, IL-12, lipoprotein of *Mycobacterium tuberculosis* acting via TLR-2, and bacterial DNA acting via TLR-9 (18, 32). There is still a possibility that an undetectable level of autocrine IFN-γ from BMmDCs can activate NOS2 expression. Moreover, innate lymphoid cells (33, 34) and NKT cells (35) could be a source of IFN-γ for activation of BCG-infected cells *in vivo* condition. However, IFN-γ requiring stimulation by adaptive immunity could not be a key player. Other members, such as IL-12, which would have a central role in early control of mycobacterial infection (6, 36-38), might be responsible for the NOS2 expression that is modulated by SOCS1. Thus, further study is needed to elucidate the detailed mechanism of NOS2 modulation via SOCS1, which is induced by BCG infection. Furthermore, we should know that other BCG strains or other *Mycobacterium* species could also utilize SOCS1 as same manner.

Taken together, our results demonstrate that induction of SOCS1 by BCG infection controls NO production by modulating NOS2 gene expression and contributes to BCG survival in the host cells that they first make contact with. Moreover, our results indicate the possibility that application of a microorganism as a modulator of the host immune system could be a powerful tool for revealing the specific function of that host factor in the context of the infectious disease.

MATERIALS AND METHODS

Mice

Specific pathogen-free C57BL/6 mice were purchased from CLEA Japan (Japan). $RAG1^{-/-}$ and $NOS2^{-/-}$ mice were purchased from Jackson Laboratory. $RAG1^{-/-}NOS2^{-/-}$ double knockout (DKO) mice were obtained by crossing $RAG1^{-/-}$ and $NOS2^{-/-}$ mice in our laboratory. Deletion of the *rag1* and *nos2* genes in all DKO mice was confirmed by PCR analysis. Genotyping was conducted using the following PCR primers: *rag1* wild, 5′- GAG GTT CCG CTA CGA CTC TG -3′; *rag1* mutant, 5′- TGG ATG TGG AAT GTG TGC GAG -3′; *rag1* common, 5′- CCG GAC AAG TTT TTC ATC GT -3′; *nos2* wild, 5′- TCA ACA TCT CCT GGT GGA AC -3′; *nos2* mutant, 5′- AAT ATG CGA AGT GGA CCT CG -3′; *nos2* common, 5′- ACA TGC AGA ATG AGT ACC GG -3′. All experiments were performed in accordance with the Guidelines for Animal Use and Experimentation, as set out by the National Institutes of Biomedical Innovation, Health and Nutrition.

Construction of rBCG

The BCG Tokyo substrain (Japan BCG Laboratory, Japan) was transformed with either the empty plasmid vector pSO246 (39) or pSO246-SOCS1DN for generation of rBCG-pSO or rBCG-SOCS1DN, respectively. The plasmid construction strategy was as follows. The HA-tagged SOCS1DN gene fragment (12) was fused with the *bla*F signal sequence gene of *Mycobacterium fortuitum* (40) and introduced downstream of the SP2 promoter (41) to generate a SOCS1DN secretion cassette. The cassette was subcloned into a *KpnII* site of the

pSO246 shuttle plasmid, generating pSO-SOCS1DN. rBCGs were grown in 7H9 broth (BD, USA) supplemented with albumin-dextrose-catalase enrichment (BD, USA), Tween-80, glycerol, and 50 μg/mL of kanamycin. rBCG cultures were used upon reaching an OD_{600} reading of 0.6 - 1.0. Existence of the SOCS1DN gene in the rBCG was confirmed by PCR analysis using the following PCR primers: *socs1* F, 5′- ATG GTA GCA CGC AAC CAG GTG -3′; *socs1* R, 5′- TCA GAT CTG GAA GGG GAA GGA -3′.

In vivo rBCG infection

Mice were inoculated intratracheally with 1×10^7 bacilli of rBCG-SOCS1DN or rBCG-pSO in 100 μL of phosphate-buffered saline (PBS) (42). rBCG cells were washed twice with PBS and then resuspended in PBS before use. rBCG-infected mice were sacrificed on days 1, 7, 14, and 28 to harvest their lungs. The lungs were homogenized in PBS containing 0.05% Tween-80. Ten-fold serial dilutions of the homogenates were plated onto 7H10 agar plates (BD, USA) supplemented with oleic acid-albumin-dextrose-catalase enrichment (BD, USA) and 50 μg/mL of kanamycin. The plates were incubated at 37°C for 3 weeks. After incubation, the bacterial burden in the lungs was calculated as log10 CFU.

Generation of bone marrow-derived dendritic cells

Mouse bone marrow-derived dendritic cells (BMmDCs) were differentiated as described previously (43). In brief, bone marrow cells were plated at 1×10^6 cells/mL in RPMI-1640 (Merck, USA) supplemented with 10 ng/mL of GM-CSF (R&D, USA) in 12-well plates with

a volume of 2 mL. On days 2 and 4, the supernatant containing nonadherent cells was removed, the wells were washed gently, and fresh medium containing GM-CSF was added. On day 6, nonadherent cells were collected, centrifuged, resuspended in a fresh medium with GM-CSF, and cultured for an additional 24 h in Petri dishes.

In vitro BCG co-cultures

Approximately 1×10^6 J774.1 cells or BMmDCs were co-cultured with rBCG at a multiplicity of infection (MOI) of 5. After 2 h incubation, the cells were washed with PBS to remove extracellular bacteria, and a fresh medium containing 50 μg/mL of gentamycin was added to each well. In a 12-well plate, the infected cells were lysed with PBS containing 0.1% Triton X-100 to determine the number of CFU or with TRIzol reagent to extract RNA for quantitative real-time RT PCR. In a 24-well plate, culture supernatants were collected for the Griess assay.

Multiplex cytokine analysis

Bronchoalveolar lavage fluid (BALF) from rBCG-infected mice was assayed for cytokine and chemokine profiles using the Bio-Plex Pro Mouse Cytokine 23-plex assay (Bio-Rad, USA) or Immunology Multiplex Assay (Merck, USA). All assays were performed according to the manufacturer's protocols.

Griess assay

Culture supernatants from rBCG-infected cells were assayed for nitrite concentration using the Griess reagent (Promega, USA) according to manufacturer's protocol. Briefly, 50 μL of each sample was added to 96-well plates and incubated with an equal volume of sulfanilamide solution for 10 min at room temperature in the dark. After another 10-min incubation with 50 μL of N-1-napthylethylenediamine dihydrochloride solution, the absorbance of each sample at 540 nm was measured. The concentration of nitrite was quantified by comparison to serially diluted $NaNO_2$ as a standard using four-parameter fit regression in the SoftMax Pro ELISA analysis software (Molecular Devices, USA).

Cell viability assay

Culture supernatants from rBCG-infected cells were assayed for LDH release using the Cytotoxicity detection kit plus (Roche Applied Science, Switzerland) according to manufacturer's protocol. Briefly, 100 μL of each sample was added to 96 well plates and incubated with 100 mL of Reaction mixture for 10 min at room temperature in the dark. Finally, 50 mL of stop solution to the wells then the absorbance of each sample at 492 nm was measured.

The BMmDC co-cultured with rBCGs were stained with SYTOX AADvance Dead cell stain kit (Thermo, USA) and analyzed with FACScanto II flow cytometer (BD biosciences, USA). Data were analyzed by FolwJo software.

Quantitative real-time RT PCR

Total RNA was isolated from rBCG-infected cells using mechanical homogenization and TRIzol reagent (In vitrogen, USA) according to the manufacturer's instructions. RNA concentrations were measured with a Nanodrop ND 1000 (Nucliber, Spain), and then Omniscript reverse transcriptase (QIAGEN, Germany) was used for cDNA synthesis. Reactions were run on an RT-PCR system (LightCycler 480; Roche Applied Science, Switzerland). Samples were normalized to β-actin and displayed as fold induction over control samples. Primers were designed using the Universal Probe Library Assay Design Center (Roche Applied Science, Switzerland), and the following primers were used: *β-actin* left, 5′-CCAACCGCGAGAAGATGA-3′; *β-actin* right, 5′- CCA GAG GCG TAC AGG GAT AG -3′; *socs1* left, 5′- GTG GTT GTG GAG GGT GAG AT -3′; *socs1* right, 5′- CCT GAG AGG TGG GAT GAG G -3′; *nos2* left, 5′- CTT TGC CAC GGA CGA GAC -3′; *nos2* right, 5′- TCA TTG TAC TCT GAG GGC TGA C -3′.

Western blotting

rBCG or rBCG-infected cells were lysed with RIPA buffer (Thermo, USA) containing a protease inhibitor cocktail (Nacalai Tesque, Japan) and phosphatase inhibitor cocktail (Nacalai Tesque, Japan). They were separated on 4-20% precast polyacrylamide gels (BIO-RAD, USA) and transferred to a PVDF membrane using the trans-blot turbo system (BIO-RAD, USA). Then the membrane was incubated overnight at 4°C with the primary antibodies anti-β-actin (1:1000; sc-47778; Santa Cruz Biotechnology, USA), anti-STAT1 (1:500; sc-346; SANTA CRUZ), anti-STAT1 phospho Y701 (1:1000; ab29045; Abcam, England),

anti-HA-tag (1:1000; ab18181; Abcam, England), anti-SOCS1 (1:2000; ab9870; Abcam, England), anti-STAT3 (1:2000; 12640S; Cell Signaling Technology, USA) and anti-STAT3 phospho Y705 (1:3000; 9145S, Cell Signaling Technology, USA). The membrane was then washed three times in Tris-buffered saline with 0.01% Tween-20 and incubated for 30 min with an HRP-conjugated secondary antibody (1:5000; 1706516; BIO-RAD, USA or 1:5000; AP180P; Merck, USA). Chemiluminescence was detected using Chemi-Lumi One Super (Nacalai Tesque, Japan). Band images were detected by ImageQuant LAS4000 (GE healthcare, USA) and band volumes were analyzed by ImageQuant TL software (GE healthcare, USA).

Histopathological Analysis

Fresh lungs were immersed in 4% buffered paraformaldehyde (PFA) overnight and then replaced in 70% ethanol before subjecting the specimen to a tissue-processing machine (Leica ASP200). The fixed specimens were automatically removed with all the water from them and replaced with paraffin wax. The paraffin-impregnated specimens were embedded in a larger block of molten paraffin (Leica EG1150H). Then the blocks were trimmed and sectioned by a microtome (Leica RM2125). Finally, the delicate sections were floated out on a water bath and picked up on a glass slide. The paraffin was dissolved from the tissue on the slide by Hemo-De (Leila) and ethanol treatment, and then the tissue was stained by hematoxylin-eosin (HE). The slides were sealed and observed under a light microscope (BX51, OLYMPUS) with appropriate magnifications.

366

367 **Transmission electron microscopy (TEM)**

368 BMmDCs infected with rBCG for transmission electron microscopy were fixed for 2 h in
369 2.5% (v/v) glutaraldehyde buffered with 0.1 M phosphate buffer, pH 7.4, at 4ºC. They were
370 post-fixed in 1% (w/v) osmium tetroxide for 1 h. The fixed specimens were washed with cold
371 phosphate buffer two times. The specimens were dehydrated in increasing concentrations of
372 ethanol followed by propylene oxide for 30 minutes and embedded in Epon 812. The blocks
373 obtained were cut using an ultramicrotome (Leica EM UC 6RT, Wetzlar, Germany) with a
374 diamond knife (DiATOME, Biel, Switzerland). The ultra-thin sections were mounted on
375 100-mesh copper grids and stained with uranyl acetate and lead citrate. The sections were
376 examined at 80 kV under a transmission electron microscope (JEM-1011; JEOL Ltd., Japan).
377 The images were processed using Gatan Microscopy Suite version 2.02.800.0.

378

379 **Statistical analysis**

380 Statistical analyses were performed using Prism 7 (GraphPad software). Statistical
381 significance was assessed using the Mann-Whitney *U* test for two group comparisons. Three
382 groups data were analyzed with Kruskal-Wallis One-way ANOVA followed by Dunn's
383 multiple comparisons test. Inherently logarithmic data from data for CFU were transformed
384 for statistical analysis. A value of $P < 0.05$ was considered significant. *, $P < 0.05$; **, $P <$
385 0.01; ***, $P < 0.001$; ns, not significant.

ACKNOWLEDGMENTS

Author contributions: S. Soma, K. Watanabe, S. Kato and Y. Yasutomi designed the research. S. Soma performed all of the experiments, with the exception of the portions indicated below. S. Mizuno and K. Matsuo constructed rBCG-SOCS1DN. S. Kawai performed transmission electron microscopy. H. Inada performed histopathological analysis. S. Soma, S. Kawai, H. Inada, K. Matsuo and Y. Yasutomi drafted the manuscript. Y. Yasutomi coordinated and directed the project.

This work was partially supported by the Japan Agency for Medical Research and Development (AMED) under Grant Number JP17fk0108007 and JP17ak0101047. The funders had no role in study design, data collection, interpretation and decision to submit this work for publication.

The authors have no commercial or financial conflict of interest.

REFERENCES

1. Stutz A, Kessler H, Kaschel ME, Meissner M, Dalpke AH. 2012. Cell invasion and strain dependent induction of suppressor of cytokine signaling-1 by Toxoplasma gondii. Immunobiology 217:28-36. https://doi.org/doi:10.1016/j.imbio.2011.08.008.
2. Zhang Y, Ma CJ, Ni L, Zhang CL, Wu XY, Kumaraguru U, Li CF, Moorman JP, Yao ZQ. 2011. Cross-talk between programmed death-1 and suppressor of cytokine signaling-1 in inhibition of IL-12 production by monocytes/macrophages in hepatitis C virus infection. J Immunol 186:3093-103. https://doi.org/doi:10.4049/jimmunol.1002006.
3. Sun K, Salmon S, Yajjala VK, Bauer C, Metzger DW. 2014. Expression of suppressor of cytokine signaling 1 (SOCS1) impairs viral clearance and exacerbates lung injury during influenza infection. PLoS Pathog 10:e1004560. https://doi.org/doi:10.1371/journal.ppat.1004560.
4. Ye S, Lowther S, Stambas J. 2015. Inhibition of reactive oxygen species production ameliorates inflammation induced by influenza A viruses via upregulation of SOCS1 and SOCS3. J Virol 89:2672-83. https://doi.org/doi:10.1128/JVI.03529-14.
5. Okumura A, Pitha PM, Yoshimura A, Harty RN. 2010. Interaction between Ebola virus glycoprotein and host toll-like receptor 4 leads to induction of proinflammatory cytokines and SOCS1. J Virol 84:27-33. https://doi.org/doi:10.1128/JVI.01462-09.
6. Carow B, Ye X, Gavier-Widen D, Bhuju S, Oehlmann W, Singh M, Skold M, Ignatowicz L, Yoshimura A, Wigzell H, Rottenberg ME. 2011. Silencing suppressor of

cytokine signaling-1 (SOCS1) in macrophages improves Mycobacterium tuberculosis control in an interferon-gamma (IFN-gamma)-dependent manner. J Biol Chem 286:26873-87. https://doi.org/doi:10.1074/jbc.M111.238287.

7. Imai K, Kurita-Ochiai T, Ochiai K. 2003. Mycobacterium bovis bacillus Calmette-Guerin infection promotes SOCS induction and inhibits IFN-gamma-stimulated JAK/STAT signaling in J774 macrophages. FEMS Immunol Med Microbiol 39:173-80. https://doi.org/doi:S0928824403002311.

8. Vazquez N, Greenwell-Wild T, Rekka S, Orenstein JM, Wahl SM. 2006. Mycobacterium avium-induced SOCS contributes to resistance to IFN-gamma-mediated mycobactericidal activity in human macrophages. J Leukoc Biol 80:1136-44. https://doi.org/doi:jlb.0306206.

9. Alexander WS, Starr R, Fenner JE, Scott CL, Handman E, Sprigg NS, Corbin JE, Cornish AL, Darwiche R, Owczarek CM, Kay TW, Nicola NA, Hertzog PJ, Metcalf D, Hilton DJ. 1999. SOCS1 is a critical inhibitor of interferon gamma signaling and prevents the potentially fatal neonatal actions of this cytokine. Cell 98:597-608. https://doi.org/doi:S0092-8674(00)80047-1.

10. Marine JC, Topham DJ, McKay C, Wang D, Parganas E, Stravopodis D, Yoshimura A, Ihle JN. 1999. SOCS1 deficiency causes a lymphocyte-dependent perinatal lethality. Cell 98:609-16. https://doi.org/doi:S0092-8674(00)80048-3.

11. Srivastava V, Manchanda M, Gupta S, Singla R, Behera D, Das G, Natarajan K. 2009. Toll-like receptor 2 and DC-SIGNR1 differentially regulate suppressors of cytokine

signaling 1 in dendritic cells during Mycobacterium tuberculosis infection. J Biol Chem 284:25532-41. https://doi.org/doi:10.1074/jbc.M109.006221.

12. Tajiri K, Imanaka-Yoshida K, Matsubara A, Tsujimura Y, Hiroe M, Naka T, Shimojo N, Sakai S, Aonuma K, Yasutomi Y. 2012. Suppressor of cytokine signaling 1 DNA administration inhibits inflammatory and pathogenic responses in autoimmune myocarditis. J Immunol 189:2043-53. https://doi.org/doi:10.4049/jimmunol.1103610.

13. Olekhnovitch R, Ryffel B, Muller AJ, Bousso P. 2014. Collective nitric oxide production provides tissue-wide immunity during Leishmania infection. J Clin Invest 124:1711-22. https://doi.org/doi:10.1172/JCI72058.

14. El Kasmi KC, Qualls JE, Pesce JT, Smith AM, Thompson RW, Henao-Tamayo M, Basaraba RJ, Konig T, Schleicher U, Koo MS, Kaplan G, Fitzgerald KA, Tuomanen EI, Orme IM, Kanneganti TD, Bogdan C, Wynn TA, Murray PJ. 2008. Toll-like receptor-induced arginase 1 in macrophages thwarts effective immunity against intracellular pathogens. Nat Immunol 9:1399-406. https://doi.org/doi:10.1038/ni.1671.

15. Chan ED, Chan J, Schluger NW. 2001. What is the role of nitric oxide in murine and human host defense against tuberculosis?Current knowledge. Am J Respir Cell Mol Biol 25:606-12. https://doi.org/doi:10.1165/ajrcmb.25.5.4487.

16. Flynn JL, Scanga CA, Tanaka KE, Chan J. 1998. Effects of aminoguanidine on latent murine tuberculosis. J Immunol 160:1796-803.

17. Bodnar KA, Serbina NV, Flynn JL. 2001. Fate of Mycobacterium tuberculosis within Murine Dendritic Cells. Infection and Immunity 69:800-809.

461 https://doi.org/doi:10.1128/iai.69.2.800-809.2001.
462 18. Davis AS, Vergne I, Master SS, Kyei GB, Chua J, Deretic V. 2007. Mechanism of
463 inducible nitric oxide synthase exclusion from mycobacterial phagosomes. PLoS
464 Pathog 3:e186. https://doi.org/doi:10.1371/journal.ppat.0030186.
465 19. Masood KI, Rottenberg ME, Carow B, Rao N, Ashraf M, Hussain R, Hasan Z. 2012.
466 SOCS1 gene expression is increased in severe pulmonary tuberculosis. Scand J
467 Immunol 76:398-404. https://doi.org/doi:10.1111/j.1365-3083.2012.02731.x.
468 20. Abdallah AM, Verboom T, Weerdenburg EM, Gey van Pittius NC, Mahasha PW,
469 Jimenez C, Parra M, Cadieux N, Brennan MJ, Appelmelk BJ, Bitter W. 2009. PPE and
470 PE_PGRS proteins of Mycobacterium marinum are transported via the type VII
471 secretion system ESX-5. Mol Microbiol 73:329-40.
472 https://doi.org/doi:10.1111/j.1365-2958.2009.06783.x.
473 21. Golby P, Nunez J, Witney A, Hinds J, Quail MA, Bentley S, Harris S, Smith N,
474 Hewinson RG, Gordon SV. 2013. Genome-level analyses of Mycobacterium bovis
475 lineages reveal the role of SNPs and antisense transcription in differential gene
476 expression. BMC Genomics 14:710. https://doi.org/doi:10.1186/1471-2164-14-710.
477 22. Siegrist MS, Unnikrishnan M, McConnell MJ, Borowsky M, Cheng TY, Siddiqi N,
478 Fortune SM, Moody DB, Rubin EJ. 2009. Mycobacterial Esx-3 is required for
479 mycobactin-mediated iron acquisition. Proc Natl Acad Sci U S A 106:18792-7.
480 https://doi.org/doi:10.1073/pnas.0900589106.
481 23. Hickman SP, Chan J, Salgame P. 2002. Mycobacterium tuberculosis induces

482 differential cytokine production from dendritic cells and macrophages with divergent
483 effects on naive T cell polarization. J Immunol 168:4636-42.
484 24. Jiao X, Lo-Man R, Guermonprez P, Fiette L, Deriaud E, Burgaud S, Gicquel B, Winter
485 N, Leclerc C. 2002. Dendritic cells are host cells for mycobacteria in vivo that trigger
486 innate and acquired immunity. J Immunol 168:1294-301.
487 25. Mohagheghpour N, van Vollenhoven A, Goodman J, Bermudez LE. 2000. Interaction
488 of Mycobacterium avium with human monocyte-derived dendritic cells. Infect Immun
489 68:5824-9.
490 26. Kuang Z, Lewis RS, Curtis JM, Zhan Y, Saunders BM, Babon JJ, Kolesnik TB, Low A,
491 Masters SL, Willson TA, Kedzierski L, Yao S, Handman E, Norton RS, Nicholson SE.
492 2010. The SPRY domain-containing SOCS box protein SPSB2 targets iNOS for
493 proteasomal degradation. J Cell Biol 190:129-41.
494 https://doi.org/doi:10.1083/jcb.200912087.
495 27. Sciorati C, Rovere P, Ferrarini M, Paolucci C, Heltai S, Vaiani R, Clementi E,
496 Manfredi AA. 1999. Generation of nitric oxide by the inducible nitric oxide synthase
497 protects gamma delta T cells from Mycobacterium tuberculosis-induced apoptosis. J
498 Immunol 163:1570-6. https://doi.org/doi:ji_v163n3p1570.
499 28. Amaral EP, Lasunskaia EB, D'Imperio-Lima MR. 2016. Innate immunity in
500 tuberculosis: how the sensing of mycobacteria and tissue damage modulates
501 macrophage death. Microbes Infect 18:11-20.
502 https://doi.org/doi:10.1016/j.micinf.2015.09.005.

503 29. Chen M, Gan H, Remold HG. 2006. A mechanism of virulence: virulent
504 Mycobacterium tuberculosis strain H37Rv, but not attenuated H37Ra, causes
505 significant mitochondrial inner membrane disruption in macrophages leading to
506 necrosis. J Immunol 176:3707-16. https://doi.org/doi:176/6/3707.
507 30. Lee J, Repasy T, Papavinasasundaram K, Sassetti C, Kornfeld H. 2011.
508 Mycobacterium tuberculosis induces an atypical cell death mode to escape from
509 infected macrophages. PLoS One 6:e18367.
510 https://doi.org/doi:10.1371/journal.pone.0018367.
511 31. Madonna S, Scarponi C, Pallotta S, Cavani A, Albanesi C. 2012. Anti-apoptotic effects
512 of suppressor of cytokine signaling 3 and 1 in psoriasis. Cell Death Dis 3:e334.
513 https://doi.org/doi:10.1038/cddis.2012.69.
514 32. Hesse M, Modolell M, La Flamme AC, Schito M, Fuentes JM, Cheever AW, Pearce EJ,
515 Wynn TA. 2001. Differential regulation of nitric oxide synthase-2 and arginase-1 by
516 type 1/type 2 cytokines in vivo: granulomatous pathology is shaped by the pattern of
517 L-arginine metabolism. J Immunol 167:6533-44.
518 33. Fuchs A, Vermi W, Lee Jacob S, Lonardi S, Gilfillan S, Newberry Rodney D, Cella M,
519 Colonna M. 2013. Intraepithelial Type 1 Innate Lymphoid Cells Are a Unique Subset
520 of IL-12- and IL-15-Responsive IFN-γ-Producing Cells. Immunity 38:769-781.
521 https://doi.org/doi:10.1016/j.immuni.2013.02.010.
522 34. Reeves RK, De Grove KC, Provoost S, Verhamme FM, Bracke KR, Joos GF, Maes T,
523 Brusselle GG. 2016. Characterization and Quantification of Innate Lymphoid Cell

524 Subsets in Human Lung. PLoS One 11:e0145961.
525 https://doi.org/doi:10.1371/journal.pone.0145961.
526 35. Godfrey DI, Stankovic S, Baxter AG. 2010. Raising the NKT cell family. Nature
527 Immunology 11:197-206. https://doi.org/doi:10.1038/ni.1841.
528 36. Holscher C, Atkinson RA, Arendse B, Brown N, Myburgh E, Alber G, Brombacher F.
529 2001. A protective and agonistic function of IL-12p40 in mycobacterial infection. J
530 Immunol 167:6957-66.
531 37. Khader SA, Partida-Sanchez S, Bell G, Jelley-Gibbs DM, Swain S, Pearl JE, Ghilardi
532 N, Desauvage FJ, Lund FE, Cooper AM. 2006. Interleukin 12p40 is required for
533 dendritic cell migration and T cell priming after Mycobacterium tuberculosis infection.
534 J Exp Med 203:1805-15. https://doi.org/doi:jem.20052545.
535 38. Miller HE, Robinson RT. 2012. Early control of Mycobacterium tuberculosis infection
536 requires il12rb1 expression by rag1-dependent lineages. Infect Immun 80:3828-41.
537 https://doi.org/doi:10.1128/IAI.00426-12.
538 39. Matsumoto S, Tamaki M, Yukitake H, Matsuo T, Naito M, Teraoka H, Yamada T. 1996.
539 A stable Escherichia coli-mycobacteria shuttle vector 'pSO246' in Mycobacterium
540 bovis BCG. FEMS Microbiol Lett 135:237-43.
541 40. Timm J, Perilli MG, Duez C, Trias J, Orefici G, Fattorini L, Amicosante G, Oratore A,
542 Joris B, Frere JM, et al. 1994. Transcription and expression analysis, using lacZ and
543 phoA gene fusions, of Mycobacterium fortuitum beta-lactamase genes cloned from a
544 natural isolate and a high-level beta-lactamase producer. Mol Microbiol 12:491-504.

545 41. Spratt JM, Britton WJ, Triccas JA. 2003. Identification of strong promoter elements of
546 Mycobacterium smegmatis and their utility for foreign gene expression in
547 mycobacteria. FEMS Microbiol Lett 224:139-42.
548 https://doi.org/doi:S0378109703004427.
549 42. Umemura M, Yahagi A, Hamada S, Begum MD, Watanabe H, Kawakami K, Suda T,
550 Sudo K, Nakae S, Iwakura Y, Matsuzaki G. 2007. IL-17-mediated regulation of innate
551 and acquired immune response against pulmonary Mycobacterium bovis bacille
552 Calmette-Guerin infection. J Immunol 178:3786-96. https://doi.org/doi:178/6/3786.
553 43. Boonstra A, Asselin-Paturel C, Gilliet M, Crain C, Trinchieri G, Liu YJ, O'Garra A.
554 2003. Flexibility of mouse classical and plasmacytoid-derived dendritic cells in
555 directing T helper type 1 and 2 cell development: dependency on antigen dose and
556 differential toll-like receptor ligation. J Exp Med 197:101-9.
557
558

559 **Figure legends**

560 **FIG 1** Construction and characterization of rBCG-SOCS1DN. (A) Whole bacterial lysates of
561 the rBCGs were collected to confirm SOCS1DN and HA-tag protein expression. WB analysis
562 was performed for every lot of rBCG, and representative data are shown. (B) Growth curves
563 of the rBCGs *in vitro*. One mg of log-phase bacteria (1 x 10^8 bacilli) was collected and
564 incubated with 25 ml of fresh 7H9 broth at 37°C, and then 100 μl was placed onto 7H10 agar
565 for counting CFU every second day. Data are representative of two independent experiments.
566 (C) To determine whether our new rBCG would induce SOCS1 expression in the host, J774.1
567 cells were co-cultured with rBCG and RNA samples were prepared for qRT-PCR. Data are
568 representative of three independent experiments. Error bars represent means ± SEM from
569 triplicate culture wells. Statistical significance of the difference from the PBS control was
570 determined by the Mann-Whitney *U* test. **, $p < 0.01$. (D) To assess the effect of SOCS1DN
571 on infected cells as level of STAT1 phosphorylation, rBCG-infected J774.1 cells were lysed
572 with RIPA buffer at indicated times. Representative data of three independent experiments are
573 shown. Each band volumes were analyzed and phosphorylation of STAT3 is presented as the
574 ratio of STAT3 phosphorylated to total STAT3.

575

576 **FIG 2** rBCG-SOCS1DN is controlled easily *in vivo*. (A) C57BL/6 and (B) $RAG1^{-/-}$ mice were
577 intratracheally inoculated with 10^7 bacilli/100 μl of BCG Tokyo, rBCG-SOCS1DN or
578 rBCG-pSO. At 1, 7, 14 and 28 days after inoculation, lungs were harvested and CFU were
579 determined. Data from two or three independent experiments were combined (n = 6-14 mice

580 at each time point). Error bars represent medians with inter-quartile range. Statistical
581 significance of three groups were analyzed with Kruskal-Wallis One-way ANOVA followed
582 by Dunn's multiple comparisons test at each time point. **, $p < 0.01$; ***, $p < 0.001$. (C) At 1
583 day and 14 days after inoculation, lung samples were also fixed for histopathological analysis
584 and then they were stained with H&E staining. Representative images from three to five mice
585 per each group are shown. Bar, 200 μm (x40); 50 μm (x200).
586
587 **FIG 3** Cytokine and chemokine profiles of BALF from rBCG-inoculated mice. (A) $RAG1^{-/-}$
588 and (B) C57BL/6 mice were intratracheally inoculated with 10^7 bacilli/100 μl of
589 rBCG-SOCS1DN or rBCG-pSO. At 1, 7, 14 and 28 days after inoculation, BALF was
590 harvested and cytokine/chemokine levels were determined by the Bio-Plex Pro mouse
591 cytokine assay. Selected cytokines/chemokines in this figure include the indicated 10 targets.
592 Data are representative of two independent experiments (n = 3 per group at each time point).
593 Error bars represent means ± SEM. Statistical significance of the difference was determined
594 by the Mann-Whitney *U* test at each time point.
595
596 **FIG 4** rBCG-SOCS1 is eliminated by host cells and induces less cell damage. Bone
597 marrow-derived myeloid dendritic cells (BMmDCs) were generated from $RAG1^{-/-}$ mice and
598 infected with rBCG-SOCS1DN or rBCG-pSO. (A) To assess viability of the rBCGs in
599 BMmDCs, CFU were determined at 0, 1, 3, 5 and 7 days after infection. Error bars represent
600 medians with inter-quartile range. Statistical significance of the difference was determined by

601 the Mann-Whitney *U* test at each time point. **, $p < 0.01$. (B) To check the total bacterial
602 number in BMmDCs, rBCG-infected cells were fixed and stained with Tb-color (Merck)
603 according to the manufacturer's protocol. About 100 individual cells at each time point were
604 examined for intracellular bacteria number. Bacterial numbers were classified into four bins: 0,
605 1-5, 6-10, and ≥11. Data are representative of two independent experiments. (C) At 3 days
606 after infection, rBCG-infected BMmDCs were fixed for transmission electron microscopy.
607 Data are representative of two independent experiments. A bar indicates 5 μm or 2 μm. To
608 determine whether there was a significant difference in cell death between
609 rBCG-SOCS1DN-infected cells and rBCG-pSO-infected cells, (D) Trypan blue staining, (E)
610 SYTOX AADvanced staining and (F) LDH release measurement were performed at indicated
611 time points. Data are representative of three independent experiments. Error bars represent
612 means ± SEM. Statistical significance of the difference from the PBS control was determined
613 by the Mann-Whitney *U* test at each time point. **, $p < 0.01$.
614
615 **FIG 5** NOS2 and NO are upregulated in rBCG-SOCS1DN-infected BMmDCs. To search for
616 the key humoral factor from BMmDCs, supernatants from rBCG-infected cells were collected.
617 (A) Cytokine/chemokine levels were determined by the Multiplex assay. Selected
618 cytokine/chemokines included 10 targets as indicated in this figure. (B) NO release levels
619 were determined by the Griess assay. (C) RNA samples from rBCG-infected BMmDCs were
620 applied for *nos2* gene real-time RT-PCR. Data are representative of two or three independent
621 experiments. Error bars represent means ± SEM. Statistical significance of the difference was

622 determined by the Mann-Whitney *U* test at each time point. **, $p < 0.01$.

623

624 **FIG 6** There is no difference in bacterial load between rBCG strains in NOS2$^{-/-}$ and DKO
625 mice. To assess the association between NOS2 expression and SOCS1 induction, C57BL/6,
626 NOS2$^{-/-}$, RAG1$^{-/-}$ and DKO mice were intratracheally inoculated with rBCG-SOCS1DN or
627 rBCG-pSO. (A) Lung samples were harvested at 1 day, 14 days and 28 days after inoculation
628 and CFU were determined. Data from two or three independent experiments were combined
629 (n = 6-19 mice at each time point). Error bars represent medians with inter-quartile range.
630 Statistical significance of the difference was determined by the Mann-Whitney *U* test at each
631 time point. *, $p < 0.05$; **, $p < 0.01$.

632

633 **FIG 7** rBCG-SOCS1DN is not controlled by BMmDCs derived from NOS2$^{-/-}$ mice. To
634 confirm that NOS2 is important to control BCG infection in the first cell the BCG makes
635 contact with, BMmDCs were generated from NOS2$^{+/+}$ (C57BL/6) and NOS2$^{-/-}$ mice and
636 infected with rBCG-SOCS1DN or rBCG-pSO. (A) To assess viability of the rBCGs in
637 BMmDCs, CFU were determined at 1 day and 7 days after infection. Error bars represent
638 medians with inter-quartile range. Statistical significance of the difference was determined by
639 the Mann-Whitney *U* test at each time point. **, $p < 0.01$; ns, not significant. (B) Images of
640 7H10 plates showing the growth of rBCGs from BMmDCs 7 days after infection. Data are
641 representative of three independent experiments.

642

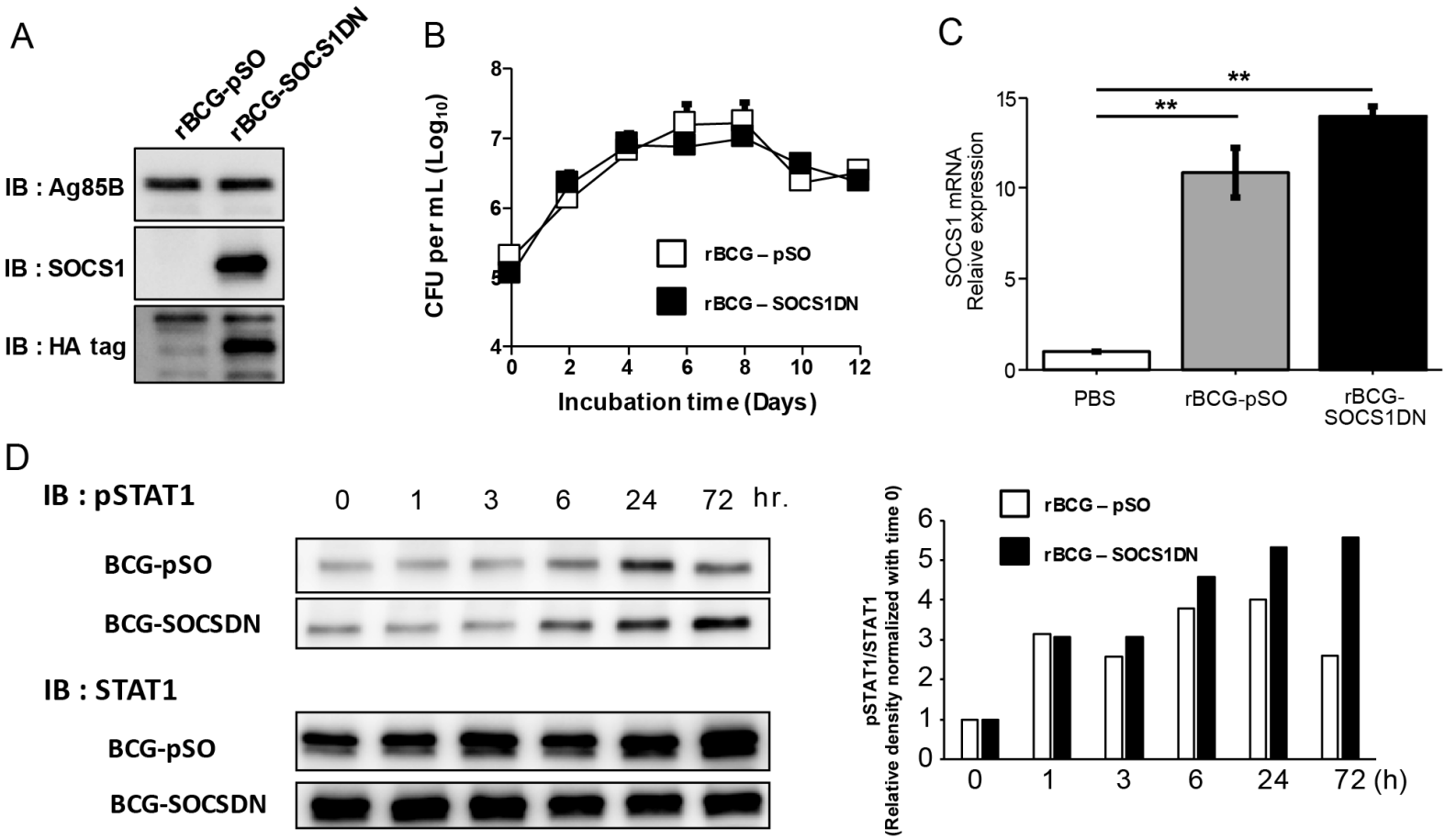
A
rBCG-pSO
rBCG-SOCS1DN
IB : Ag85B
IB : SOCS1
IB : HA tag
B
CFU per mL (Log10)
Incubation time (Days)
rBCG – pSO
rBCG – SOCS1DN
C
SOCS1 mRNA
Relaive expression
**
**
PBS
rBCG-pSO
rBCG-SOCS1DN
D
IB : pSTAT1
0 1 3 6 24 72 hr.
BCG-pSO
BCG-SOCSDN
IB : STAT1
BCG-pSO
BCG-SOCSDN
pSTAT1/STAT1
(Relative density normalized with time 0)
rBCG – pSO
rBCG – SOCS1DN
0 1 3 6 24 72 (h)

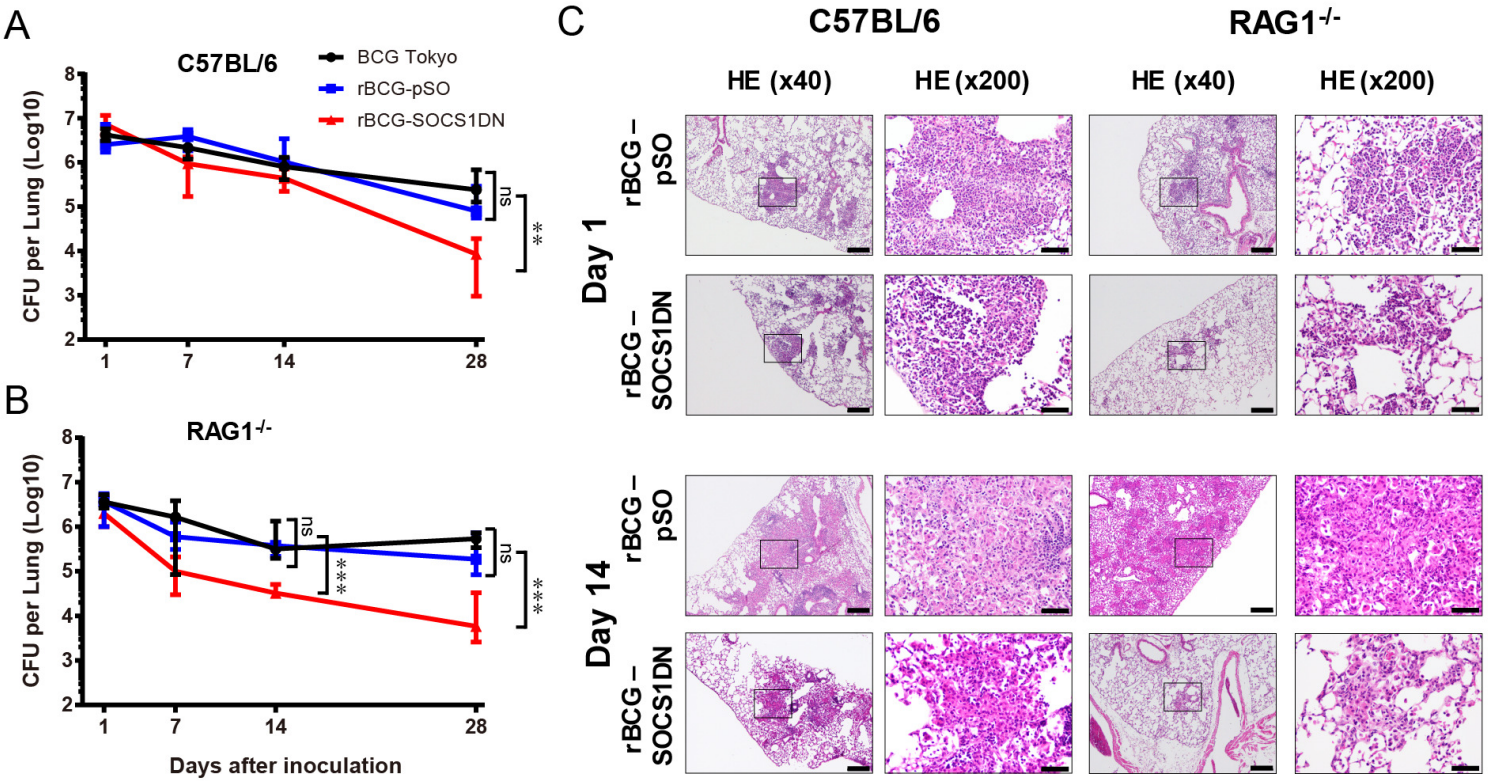
A
C57BL/6
BCG Tokyo
rBCG-pSO
rBCG-SOCS1DN
CFU per Lung (Log10)
ns
**
B
RAG1-/-
ns
***
***
Days after inoculation
C
C57BL/6
RAG1-/-
HE (x40)
HE (x200)
HE (x40)
HE (x200)
Day 1
rBCG – pSO
rBCG – SOCS1DN
Day 14
rBCG – pSO
rBCG – SOCS1DN

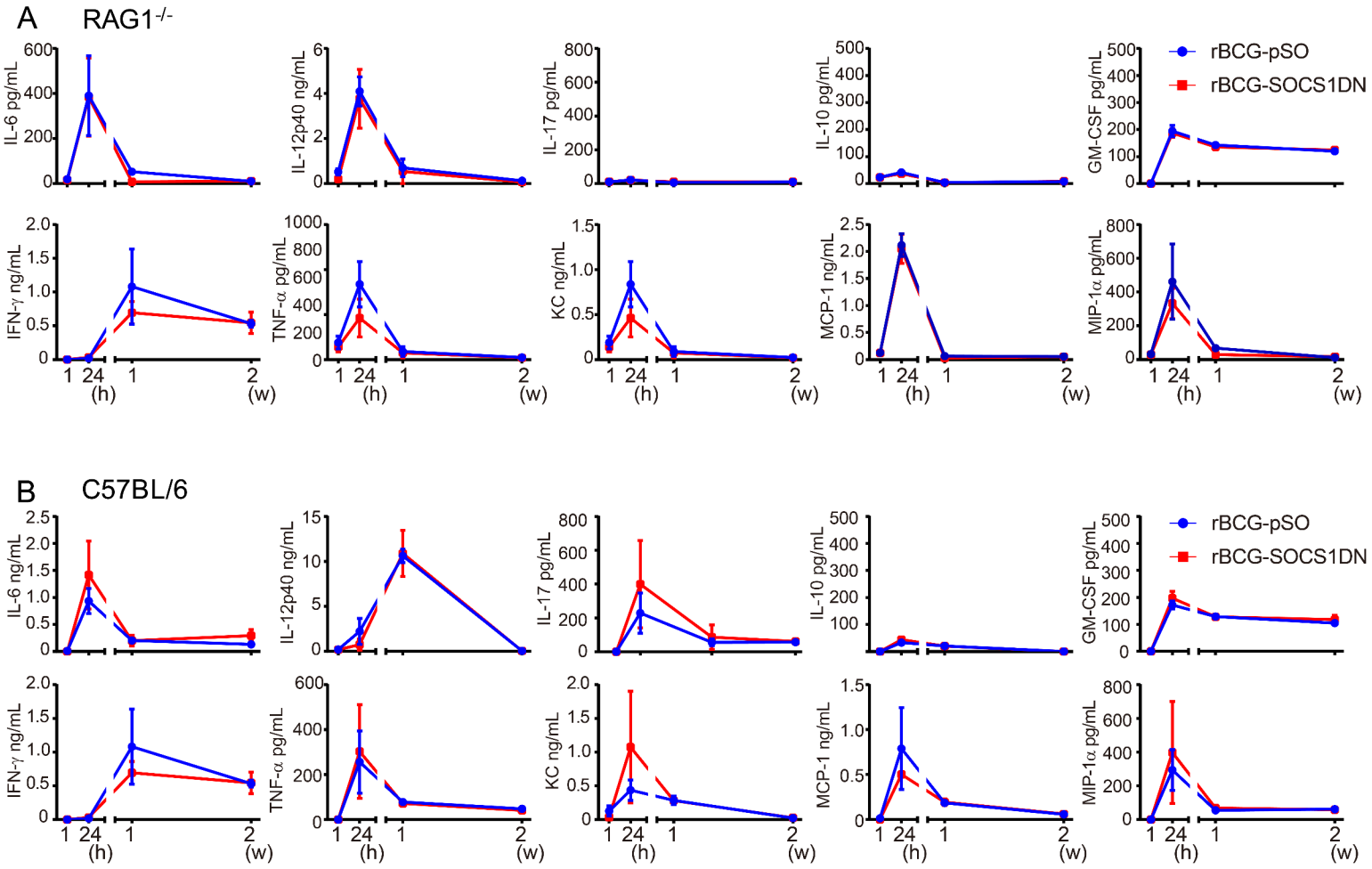
A
RAG1-/-
IL-6 pg/mL
IL-12p40 ng/mL
IL-17 pg/mL
IL-10 pg/mL
GM-CSF pg/mL
rBCG-pSO
rBCG-SOCS1DN
IFN-γ ng/mL
TNF-α pg/mL
KC ng/mL
MCP-1 ng/mL
MIP-1α pg/mL
1 24 1 2
(h) (w)
B
C57BL/6
IL-6 ng/mL
IL-12p40 ng/mL
IL-17 pg/mL
IL-10 pg/mL
GM-CSF pg/mL
rBCG-pSO
rBCG-SOCS1DN
IFN-γ ng/mL
TNF-α pg/mL
KC ng/mL
MCP-1 ng/mL
MIP-1α pg/mL
1 24 1 2
(h) (w)

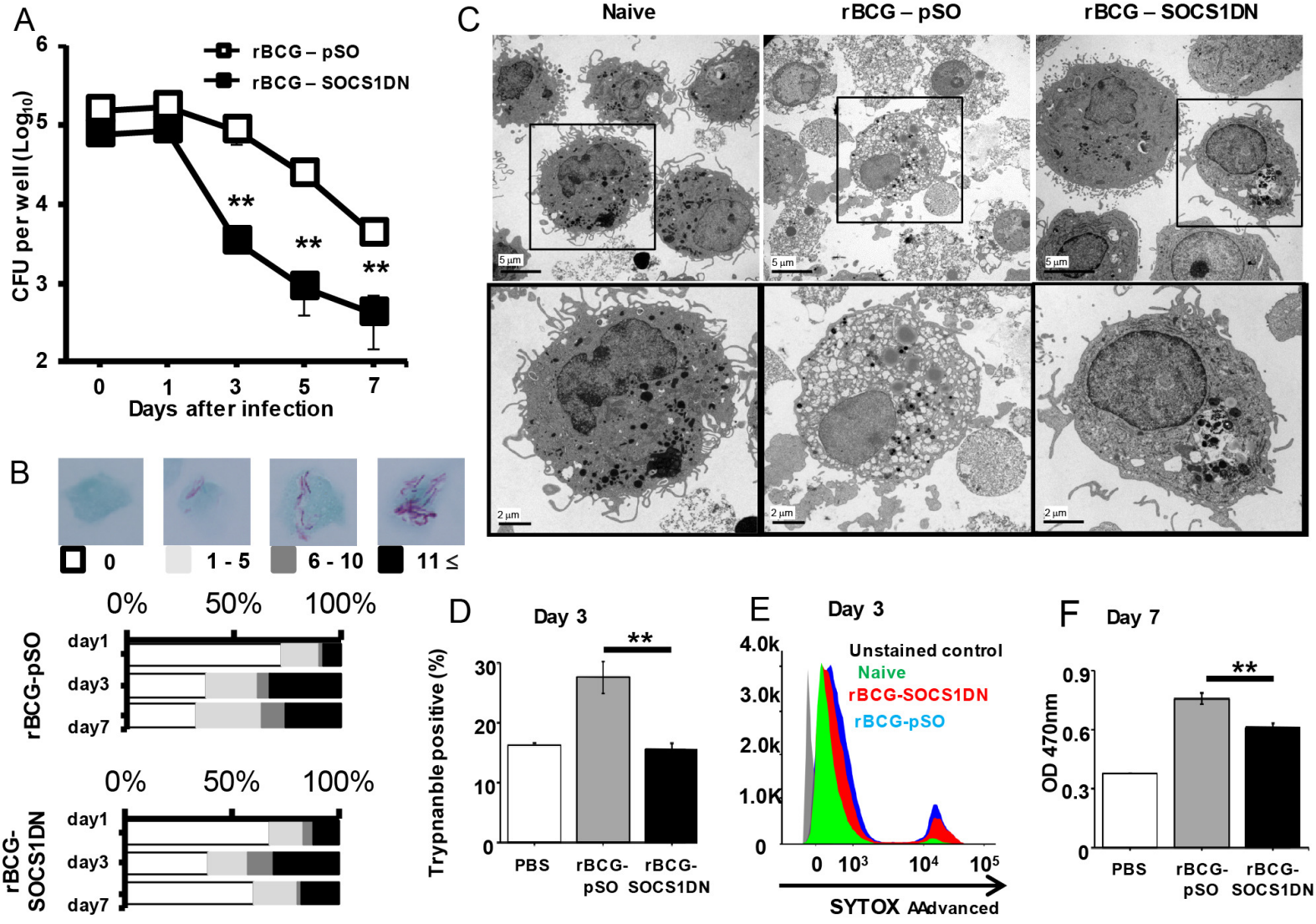
A
rBCG – pSO
rBCG – SOCS1DN
CFU per well (Log10)
Days after infection
**
B
0
1 - 5
6 - 10
11 ≤
0%
50%
100%
day1
day3
day7
rBCG-pSO
rBCG-SOCS1DN
C
Naive
rBCG – pSO
rBCG – SOCS1DN
5 μm
2 μm
D
Day 3
Trypnanble positive (%)
PBS
rBCG-pSO
rBCG-SOCS1DN
E
Day 3
Unstained control
Naive
rBCG-SOCS1DN
rBCG-pSO
SYTOX AAdvanced
F
Day 7
OD 470nm

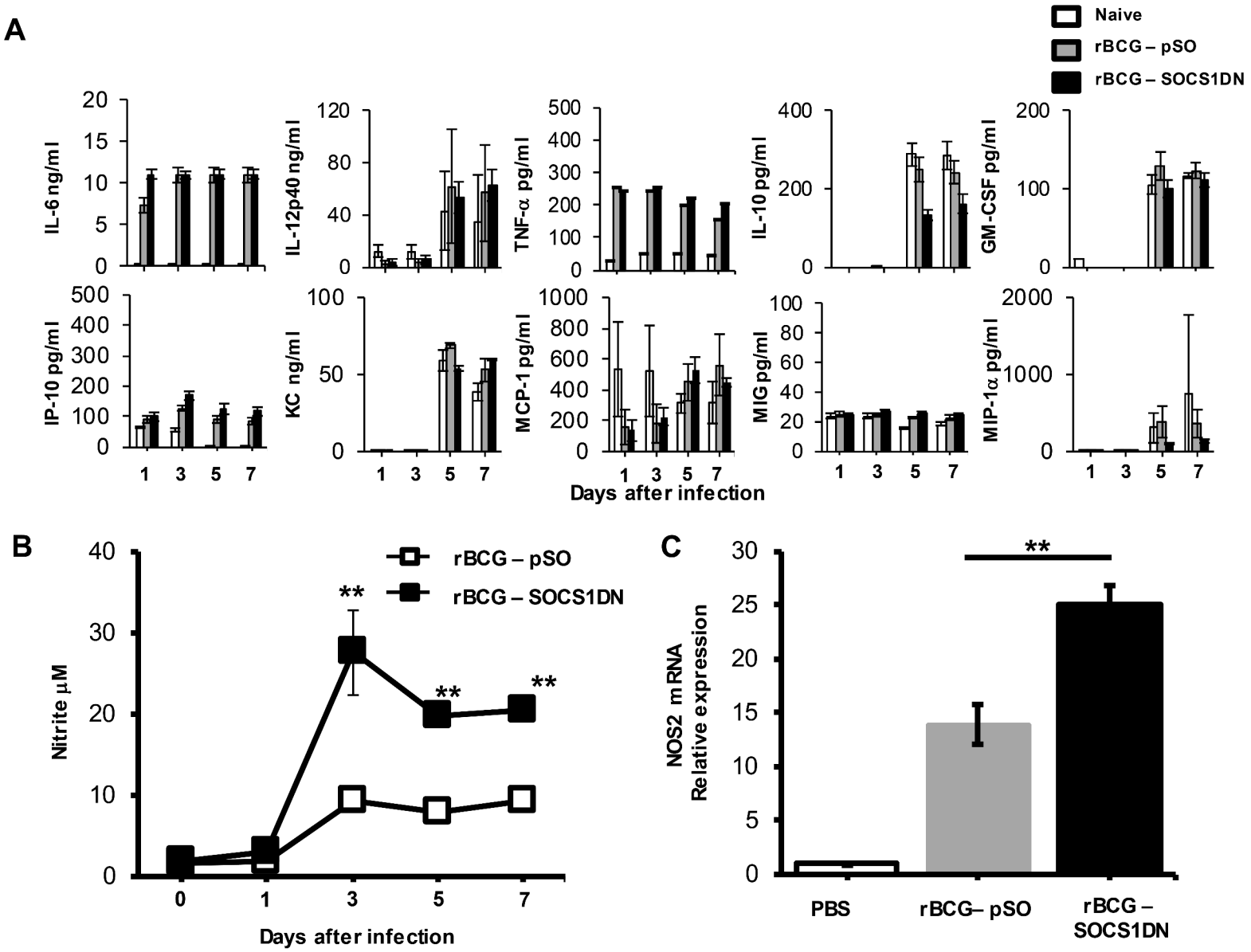
A
Naive
rBCG – pSO
rBCG – SOCS1DN
IL-6 ng/ml
IL-12p40 ng/ml
TNF-α pg/ml
IL-10 pg/ml
GM-CSF pg/ml
IP-10 pg/ml
KC ng/ml
MCP-1 pg/ml
MIG pg/ml
MIP-1α pg/ml
Days after infection
B
rBCG – pSO
rBCG – SOCS1DN
Nitrite μM
Days after infection
C
NOS2 mRNA Relative expression
PBS
rBCG– pSO
rBCG – SOCS1DN

A

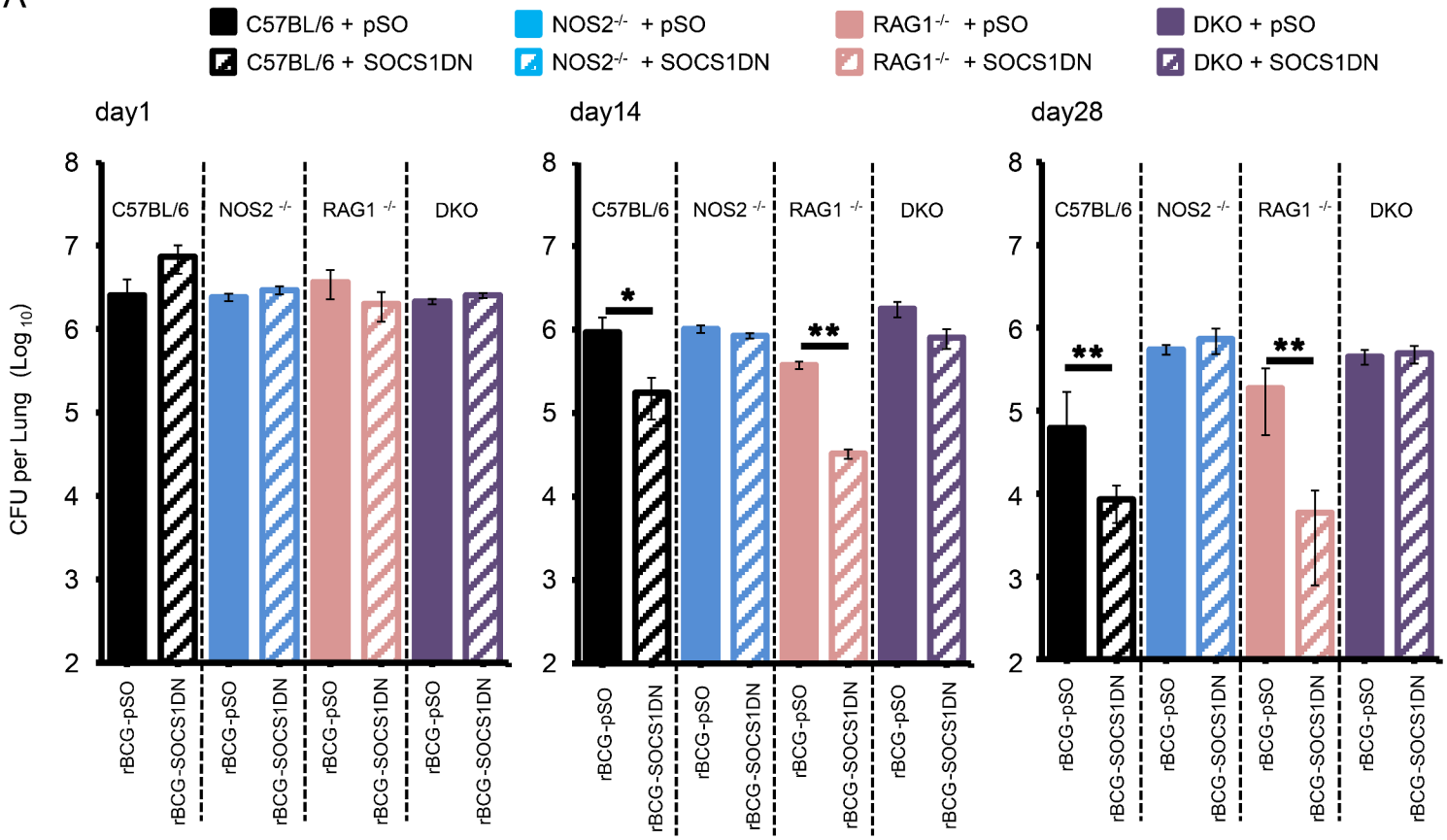
C57BL/6 + pSO
C57BL/6 + SOCS1DN
NOS2-/- + pSO
NOS2-/- + SOCS1DN
RAG1-/- + pSO
RAG1-/- + SOCS1DN
DKO + pSO
DKO + SOCS1DN
day1
day14
day28
CFU per Lung (Log10)
C57BL/6
NOS2 -/-
RAG1 -/-
DKO
rBCG-pSO
rBCG-SOCS1DN
*
**

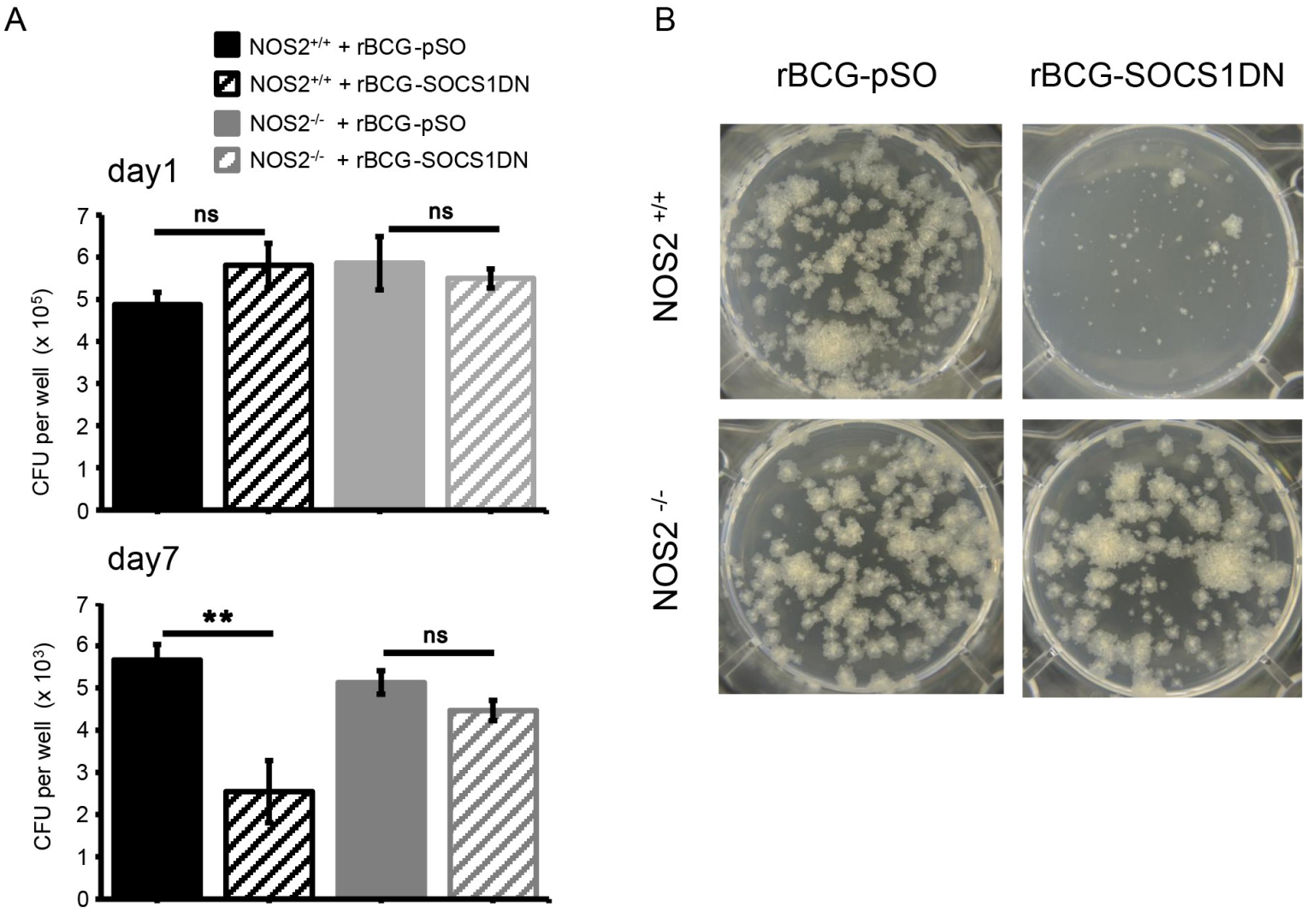
A
NOS2+/+ + rBCG-pSO
NOS2+/+ + rBCG-SOCS1DN
NOS2-/- + rBCG-pSO
NOS2-/- + rBCG-SOCS1DN
day1
CFU per well (x 10^5)
ns
ns
day7
CFU per well (x 10^3)
**
ns
B
rBCG-pSO
rBCG-SOCS1DN
NOS2 +/+
NOS2 -/-